CHARACTERISATION OF LINEAR AND NON-LINEAR OPTICS OF THE SOLARIS STORAGE RING

W. Wiatrowska*, J. Biernat, R. Panas, A.I. Wawrzyniak
SOLARIS National Synchrotron Radiation Centre, Krakow, Poland

Abstract

This work presents a comprehensive characterization of the linear and non-linear optics of the SOLARIS storage ring under various operational conditions, including post-shutdown recovery and routine operation. Long-term studies were conducted using key diagnostic systems: the Bunch-by-Bunch Feedback (BBBF) system, LUMOS visible-light diagnostics, the PINHOLE X-ray beamline, and Turn-by-Turn (TBT) data from Libera Brilliance+. Measurements focused on fundamental machine parameters such as dispersion, beta functions, working point, chromaticity, synchrotron tune, and emittance, as well as the influence of insertion devices. Additionally, the impact of harmonic cavity settings, filling patterns, and chromaticity adjustments on emittance, bunch length, and beam lifetime was investigated. These results provide essential insights for optimizing beam quality, stability, and operational efficiency to enhance user performance at SOLARIS.

INSTRUMENTATION AND ALGORITHMS

Reference diagnostic measurements were typically taken under the standard storage ring magnets configurations with operating energy 1.5 GeV and full filling pattern of 32 bunches. The maximum current was typically 50 mA, to minimize Landau contribution in the measurement, and therefore cavity power was typically set at 110–120 mV. The insertion devices (IDs) were kept open unless evaluating undulator impact. Correctors (horizontal and vertical), used during LOCO measurement, apply a kick delta of (respectively) 4.51 A and 3.83 A

WARMING UP OF THE STORAGE RING

As the storage ring reaches its target temperature, the main RF frequency is automatically lowered in time to the default level, shifting the orbit diameter inversely. Consequently, the Master Oscillator (MO) frequency serves as a critical parameter for evaluating optics quality.

The main RF frequency is being constantly monitored and archived, thus one may easily retrieve the data from any period within 10 years. The Figure 1 shows data from days before, and three months after three last shutdowns.

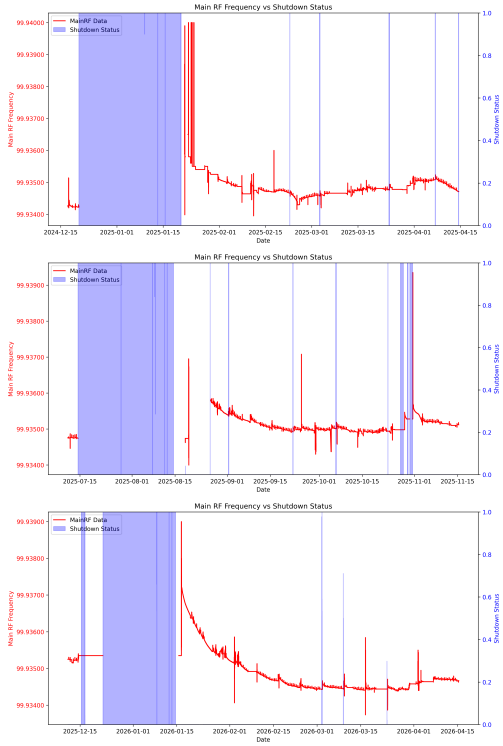

Figure 1: Visualization of changing orbit of the beam in storage ring represented by differs in Main RF frequency (red) with highlighted shutdown status of the ring (blue)

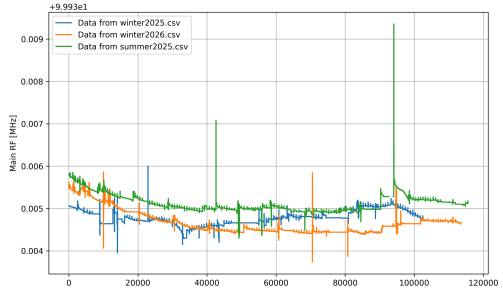

Figure 2: Comparison of Main RF frequency from last three shutdowns.

Figure 2 presents a comparison of these datasets on a single plot. It is clearly visible that the main RF frequency since the latest shutdown is significantly lower than in any previous run. This shift can likely be attributed to the increased temperature of the cooling water. Furthermore, a subsequent increase in the Master Oscillator (MO) frequency is observable, corresponding to the point when the temperature was restored to its nominal value.

* wiktoria01wiatrowska@gmail.com

IMPACT OF THE IDS

It is well-established that insertion devices (IDs) have a significant impact on the electron beam dynamics.

Although dedicated correction tables are implemented to compensate for the magnetic field errors of each device, the residual impact remains visible, especially at minimum gaps and maximum phase settings. Consequently, LOCO measurements were performed for every combination of insertion device positions to quantify these effects.

All other storage ring parameters were maintained at the standard operating conditions. These measurements allow for a systematic evaluation of the tune shift and β-beating induced by each ID (Figure 3), providing the necessary data to refine the active compensation strategies.

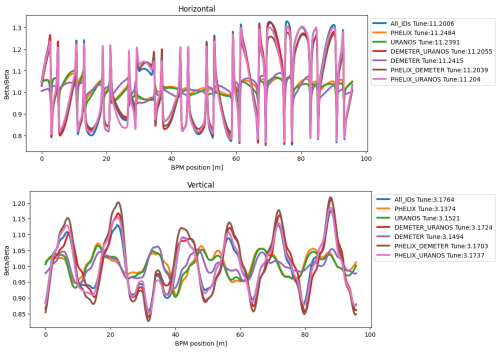

Figure 3: The beta beating for different insertion devices configurations

For configurations with a single ID, the beta-beating ratio approaches unity, indicating that the measured beta functions for these specific states are in close agreement with the ideal lattice model. While the horizontal beta-beating remains relatively stable throughout most of the ring, the section between 25 m and 45 m—corresponding to the location of the insertion devices exhibits significant deviations. A closer look at the beta and dispersion functions in this section is presented in Figure 4.

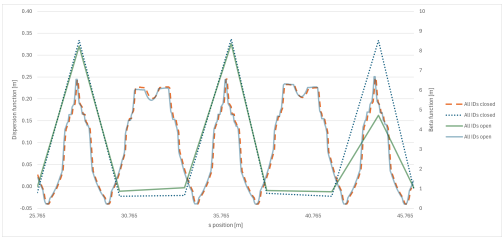

Figure 4: Dispersion and beta functions with opened and closed insertion devices

The tune itself is also connected to insertion devices in storage ring. Due to vertical focusing of the undulator, the vertical tune changes along with the equation 1:

$$\Delta\nu_y \approx \frac{L\langle\beta_y\rangle K^2}{2\lambda_u^2\gamma^2} \tag{1}$$

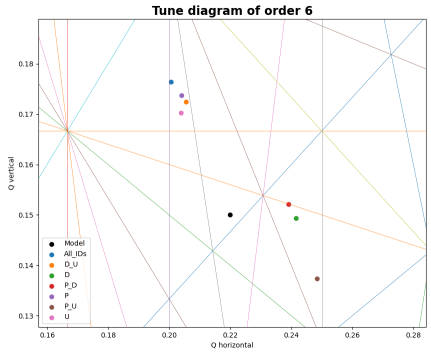

Figure 5: Tune values for insertion devices configurations

On Figure 5 it is perfectly visible that each of the undulator adds it's part to this tune shift. The more undulators are included in measurement, the further the tune is shifted against the model value.

Configuration	ν_V
PHELIX	0.1374
DEMETER	0.1494
URANOS	0.1521
PHELIX & DEMETER	0.1703
DEMETER & URANOS	0.1724
PHELIX & URANOS	0.1737
All IDs	0.1764

Table 1: tabular representation of sorted vertical partial tune values for insertion devices configurations

From the sorted tabular representation of data in Table 1, one might assume that Uranos is the most influential insertion device regarding tune. Only configurations including the Uranos undulator are located near the most extreme data point. Their exact values suggest that the second most impactful device is the Phelix undulator. To confirm this, it is necessary to examine the single undulator configurations. Here, Phelix also takes second place, as Demeter barely changes the vertical tune.

TUNE AND WORKING POINT MEASUREMENT

Tune Shift

Since energy shifts lead to tune shifts, monitoring the working point across different settings is crucial. Measurements were performed during the energy ramping process, where the beam energy was increased from 0.5 GeV to 1.5 GeV, with plunger movement occurring at 1.1 GeV. All parameters were kept at standard operating levels, except for the current, which was increased to 100 mA to enhance the impact of Landau damping.

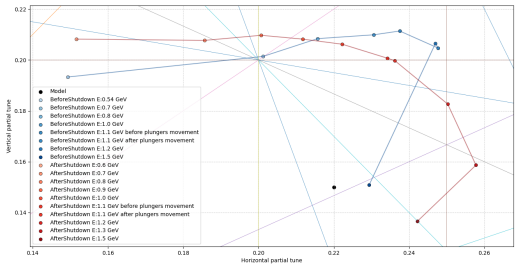

Figure 6: Tune shift during the beam energy ramping process, comparing data from after (red) and before (blue) the shutdown.

The results presented in Figure 6 show a significant discrepancy between the data collected before and after the shutdown. A substantial shift of the working point at full energy compared to the theoretical model is also observed. Furthermore, the data-point lies on a 5th-order resonance, which may cause additional disturbances in the beam spectrum.

Establishing a Stable Working Point

During commissioning, it was observed that the horizontal tune deviated significantly from the theoretical design values, resulting in beam instabilities. To address this, a systematic optimization process was conducted to shift the working point toward a more stable region. The optimization utilized the inner and outer combined sextupole-quadrupole magnets (SQF_i, SQF_o) and the Pole Face Strips (PFS).

To determine the control strategy, the response of the tunes to changes in magnet currents was mapped (Table 2).

Table 2: Measured tune sensitivities to magnet current adjustments.

Magnet	Current Change	$\Delta\nu_H$	$\Delta\nu_V$
SQF_i	455.5 A $\rightarrow$ 454.3 A	-0.025	+0.019
SQF_o	1.34 A $\rightarrow$ 1.88 A	+0.020	-0.015
PFS	0.5 A $\rightarrow$ 1.5 A	~0.000	+0.030

By applying these experimentally derived sensitivities, the beam was successfully steered to a new working point. As shown in Table 3, the final parameters demonstrate excellent agreement with the theoretical model.

Table 3: Comparison of initial, optimized, and theoretical working points.

Configuration	ν_H	ν_V
Measured (Initial)	0.24224	0.13664
Measured (Optimized)	0.22022	0.15065
Design Model	0.22000	0.15000

EMITTANCE AND LIFETIME

Understanding the impact of both passive and active cavity voltages on bunch length, lifetime, and emittance is crucial for maintaining a stable working point. To investigate these dependencies, measurements were conducted for two distinct operating modes: first, as a function of beam current decay with a constant RF voltage ratio of approximately 2.7 (Figures 7,8), and second, by varying the RF ratio while maintaining a near-constant current (Figures 9, 10).

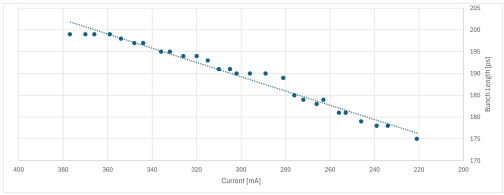

Figure 7: Bunch length as a function of beam current decay.

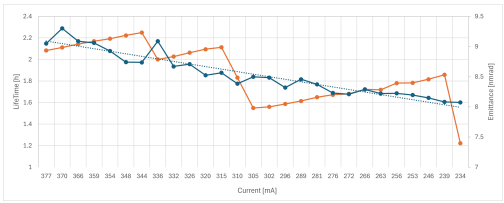

Figure 8: Emittance (blue) and lifetime (orange) measured during current decay.

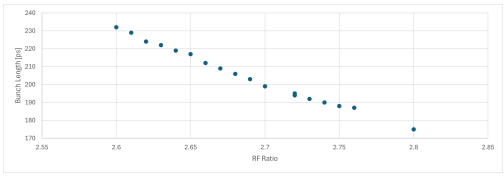

Figure 9: Impact of the RF voltage ratio on bunch length.

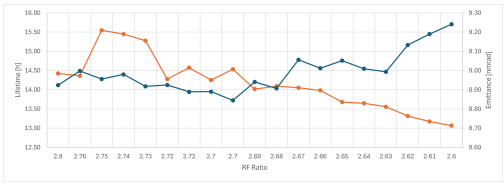

Figure 10: Emittance (blue) and lifetime (orange) as a function of the RF voltage ratio.

The observed trends are consistent across both operating modes. As the beam current decays, both the bunch length and emittance decrease significantly. The RF ratio exhibits the opposite effect: a lower ratio results in a longer bunch and increased emittance.

SUMMARY

The comprehensive measurements and characterization of the SOLARIS storage ring optics presented in this work underscore the vital importance of systematic machine studies. By utilizing advanced diagnostic tools, established a robust baseline for both linear and non-linear beam dynamics. These studies are not merely a technical necessity but a fundamental requirement for maintaining high-quality research conditions.

ACKNOWLEDGMENTS

The work is supported under the Polish Ministry and Higher Education project: "Support for research and development with the use of research infrastructure of the National Synchrotron Radiation Centre SOLARIS" under contract nr 1/SOL/2021/2.

REFERENCES

[1] A.I. Wawrzyniak *et al.*, "Solaris a new class of low energy and high brightness light source", *Nucl. Instrum. Methods Phys. Res., Sect. B*, vol. 411, pp. 4–11, 2017. doi:10.1016/j.nimb.2016.12.046

[2] A.I. Wawrzyniak, C.J. Bocchetta, S.C. Leemann, and M. Eriksson, "Solaris Storage Ring Lattice Optimisation with Strong Insertion Devices", in *Proc. IPAC'12*, New Orleans, LA, USA, May 2012, paper TUPPC037, pp. 1164–1166.

[3] H. Wiedemann, *Particle Accelerator Physics*, 3rd ed., Berlin, Germany: Springer-Verlag, 2007.